Supplementary Material

High intrinsic carrier mobility and photon absorption in perovskite $CH_3NH_3PbI_3$

Youwei Wang,[1] Yubo Zhang,[1] Peihong Zhang,[2] Wenqing Zhang[1,3*]

[1]*State Key Laboratory of High Performance Ceramics and Superfine Microstructures, Shanghai Institute of Ceramics, Chinese Academy of Sciences, Shanghai 200050, China*

[2]*Department of Physics, University at Buffalo, SUNY, Buffalo, New York 14260, USA*

[3]*Materials Genome Institute, Shanghai University, Shanghai 200444, China*

*Corresponding author. Email: wqzhang@mail.sic.ac.cn

1. Band structures

It is well recognized that the spin-orbit coupling (SOC) is crucial for the band structure calculation of $CH_3NH_3PbI_3$.[1] We also calculated the band structure of orthorhombic $CH_3NH_3PbI_3$ using the Perdew-Burke-Ernzerh (PBE) functional without and with the SOC effect, as shown in Fig. S1 (a) and (b). The two band structures are aligned with the organic states, e.g., C-2*p* states around −5.0 eV below the valence band maximum (VBM) state, of which the SOC effect is neglectable. While the top of valence band undergoes limited changes, radical change is found at the bottom of conduction band. Specifically, the conduction band minimum (CBM) and VBM shifts are 0.86 and 0.18 eV, respectively, after including the SOC effect in the calculations. To understand the difference, it should be noticed that the CBM is solely from the Pb-6p states, but the VBM is from hybridized I-5*p* and Pb-6*s* states. The energy shift of Pb-6p states owing to SOC effect is much heavier than the I-5p states. Moreover, compared with the energy shifts of Pb-6p and I-5p states depending on the SOC effect, the Pb-6s states have negligible response to the SOC effect and, thus, the anti-bonding states of Pb-6s and I-5p further reduce the energy shift of VBM state. As a result, after the SOC effect considered in the calculation, the energy shift of CBM state is four times bigger than the VBM state.

The modified Becke-Johnson (mBJ) potential is well-known for its reliable prediction of both bandgaps and band topologies for narrow-gap semiconductors, especially for simple *sp*-hybridization systems.[2] We also calculated the results from this functional, as shown in Fig. S1 (c) and (d). As expected, the overall band structures are quite similar from the PBE and mBJ functional, although the bandgaps are significantly improved within the mBJ potential. The comparison with experimental bandgaps will be given in the following section.

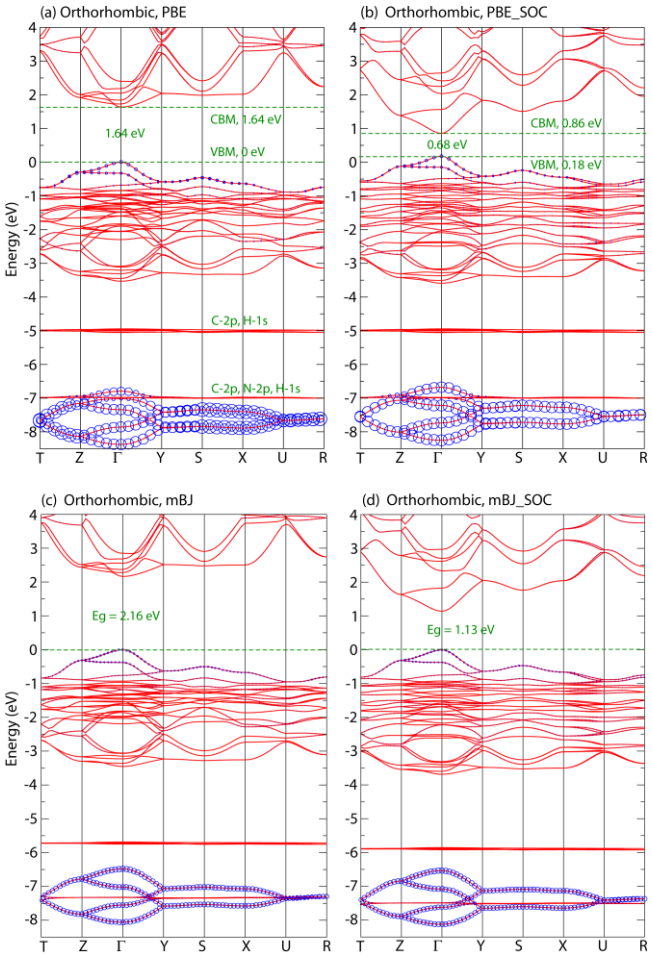

Fig. S1. Band structures of orthorhombic $CH_3NH_3PbI_3$: (a) PBE without SOC effect, (b) PBE with SOC effect, (c) mBJ without SOC effect, and (d) mBJ with SOC effect. The band structures with and without the SOC effect are compared by aligning the deep-lying organic states. The Pb-6*s* wave function is projected onto the band structures. The dispersion curves for the three phases are shown along the following directions of T(-½,0,½) → Z(0,0, ½) → Γ(0,0,0) → Y(-½,0,0) → S(-½,½,0) → X(0, ½,0) → U(0, ½, ½) → R(½,½,½). The VBMs are set to be zero.

2. Structural influence on the bandgap

The bandgap of $CH_3NH_3PbI_3$ is calculated to be around 1.1 ~ 1.3 eV from the mBJ functional with the SOC effect included for tetragonal and orthorhombic phases (see Table S1). The result seems to be still underestimated compared with the experimental values of 1.5 ~ 1.7 eV,[3-6] which is in contrast to the observation that the mBJ works well for bandgap of *sp*-hybridization semiconductors. In fact, such "underestimation" was also observed for the many-body correction in the form of G0W0 calculation.[7,8] We argued that there are two possible issues tend to affect the straightforward comparison between the theoretical and experimental results.

Table S1. Bandgaps (eV) of $CH_3NH_3PbI_3$ from experimental measurement and theoretical calculations

	Orthorhombic	Tetragonal	Pseudo-Cubic
Experiments	1.68-1.72[a]	1.5-1.6[b]	
PBE, without SOC	1.64	1.86	1.29
PBE, with SOC	0.68	0.83	0.18
mBJ, without SOC	2.16	2.37	1.81
mBJ, with SOC	1.13	1.27	0.67

a reference 3,4
b reference 5,6

Firstly, the bandgap of $CH_3NH_3PbI_3$ can be sensitively influenced by the structural properties. As discussed in our article (see Section 3.4), the effective masses of band-edge states sensitively rely on the Pb-I bonding length,

which in turn is strongly depended on the thermodynamic movement of $CH_3NH_3^+$ organic base. It is obvious that bandgap has a strong dependence on the temperature. Experimentally, the measured structures at finite temperature (such as the cubic phase) give the average atomic positions, which undergo strong dynamic movement induced by the thermal movement of the organic base. It is quite possible that, for example, the cubic structure also contains strongly deformed PbI_6 octahedra (and thus distorted Pb-I bond lengths) in practice, although the lattice parameters remain unchanged. However, this temperature effect is not fully or accurately considered in our current work. So, the crystal structure properties should be carefully investigated for a reliable prediction of the bandgap.

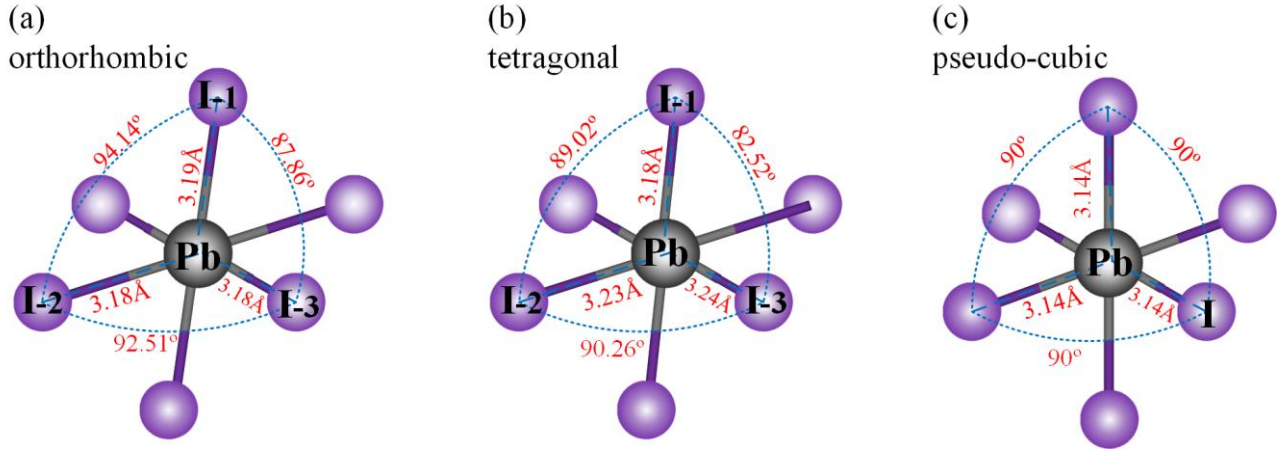

Fig. S2. Local PbI_6 octahedra of (a) orthorhombic, (b) tetragonal and (c) pseudo-cubic $CH_3NH_3PbI_3$. The average Pb-I bond lengths in a PbI_6 octahedron are 3.18, 3.22, and 3.14 Å for the orthorhombic, tetragonal, and pseudo-cubic structures, respectively.

Secondly, the practical issue is about the phase mixing or defects in $CH_3NH_3PbI_3$. It is found that $CH_3NH_3PbI_3$ sample is sensitive to moisture and tends to decompose into PbI_2 (and CH_3NH_2, HI),[9] which has a much greater bandgap of 2.3 eV.[10-12] So, we argued that the phase mixing with PbI_2 can contribute to bandgap overestimation experimentally. In fact, similar effect has been found in $Cu_2ZnSnSe_4$, of which the bandgap had been strongly overestimated due to the mixing with a secondary phase of ZnSe.[13]

3. Band shift with volume dilation

Deformation potential is the shift of site energies with respect to the volume dilation. So, it is helpful to firstly investigate the properties of band-edge states. The case for the CBM is quite simple, i.e., it is from anti-bonding states between Pb-6p and I-5p orbitals. The upper valence band is mainly composed of three types of states, i.e., bonding states from Pb-6p and I-5p orbitals coupling, anti-bonding states from inter-site Pb-6s and I-5p coupling, and anti-bonding states from intra-site Pb-6s and Pb-6p coupling. The last two couplings are typical interactions in systems with "lone pairs", such as PbO.[14] We noticed that the lone pair effect causes *abnormal* VBM deformation potential in $CH_3NH_3PbI_3$. Because the intra-site hybridization will be seldom influenced by the volume dilation, we only focus on the inter-site item in following discussions.

Table S2. Contributions to the shifts of the VBM and CBM site energies in $CH_3NH_3PbI_3$ and ZnS with volume dilation. The ↑ and ↓ arrows mean that the energetic items are shifted upwardly and downwardly, respectively, upon dilation. The × means no effect.

		VBM	CBM
$MAPbI_3$	Kinetic energy	↓	↓
	Pb-6p, I-5p	↑ (Bonding)	↓ (Anti-bonding)
	Pb-6s, I-5p	↓ (Anti-bonding)	× (No states)
	Pb-6s, Pb-6p	× (Anti-bonding)	× (No states)
ZnS	Kinetic energy	↓	↓
	Zn-4s, S-3p	↑ (Bonding)	↓ (Anti-bonding)
	Zn-3d, S-3p	↓ (Anti-bonding)	× (No states)

The responses of dominant energetic items that contribute to the VBM and CBM positions in $CH_3NH_3PbI_3$ upon dilation are shown in Table S2 and Fig. S3. The kinetic energy, which is proportional to $1/l^2$ (l is the cation-anion bond length), becomes smaller for all the states. Another item contributes to the CBM is the anti-bonding between Pb-6p and I-5p states and it goes downwardly upon dilation. As a result, the deformation potential of the CBM is quite strong, as usually found in other semiconductors like ZnS.[15] However, our calculation shows that the VBM site energy has a much stronger response to the dilation, which is ascribed to the anti-bonding item from hybridization between Pb-6s and I-5p orbitals.

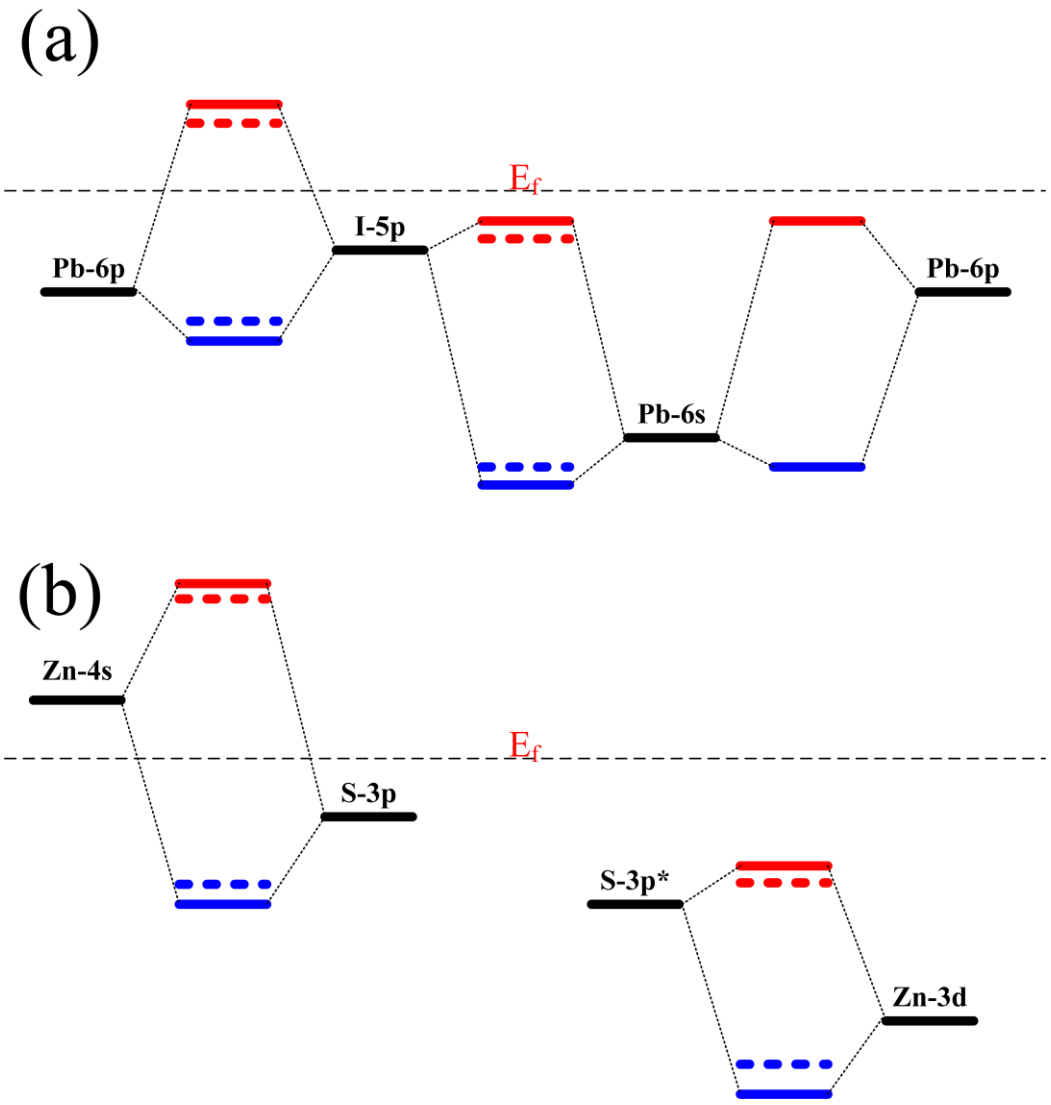

Fig. S3. Schematic diagrams of chemical bonding in (a) $CH_3NH_3PbI_3$ and (b) ZnS. The red and blue solid/dashed lines represent the anti-bonding and bonding states, respectively. The dashed lines show the energy shift with volume dilation.

Reference

1 J. Even, L. Pedesseau, J. M. Jancu and C. Katan, J. Phys. Chem. Lett., 2013, **4**, 2999-3005.

2 D. Koller, F. Tran and P. Blaha, Phys. Rev. B, 2011, **83**, 195134.

3 T. Ishihara, J. Lumin., 1994, **60-61**, 269-274.

4 G. C. Papavassiliou, I. B. Koutselas, Synth. Met., 1995, **71**, 1713-1714.

5 T. Baikie, Y. Fang, J. M. Kadro, M. Schreyer, F. Wei, S. G. Mhaisalkar, M. Graetzel and T. J. White, J. Mater. Chem. A, 2013, **1**, 5628-5641.

6 J. H. Noh, S. H. Im, J. H. Heo, T. N. Mandal and S. I. Seok, Nano Lett., 2013, **13**, 1764-1769.
7 P. Umari, E. Mosconi and F. De Angelis, Sci. Rep., 2014, **4**, 4467.
8 F. Brivio, K. T. Butler, A. Walsh and M. van Schilfgaarde, Phys. Rev. B, 2014, **89**, 155204.
9 J. M. Frost, K. T. Butler, F. Brivio, C. H. Hendon, M. van. Schilfgaarde and A. Walsh, Nano Lett., 2014, **14**, 2584–2590
10 A. Ferreira da Silva, N. Veissid, C.Y. An, I. Pepe, N. Barros de Oliveira and A.V. Batista da Silva, Appl. Phys. Lett., 1996, **69**, 1930.
11 T. Supasai, N. Rujisamphan, K. Ullrich, A. Chemseddine and T. Dittrich, Appl. Phys. Lett., 2013, **103**, 183906.
12 D. S. Ahlawat, Mod. Phys .Lett. B, 2012, **26**, 8.
13 S. Ahn, S. Jung, J. Gwak, A. Cho, K. Shin, K. Yoon, D. Park, H. Cheong and J. H. Yun, Appl. Phys. Lett., 2010, **97**, 021905.
14 D. Payne, R. Egdell, A. Walsh, G. Watson, J. Guo, P. A. Glans, T. Learmonth and K. Smith, Phys. Rev. Lett., 2006, **96**, 157403
15 S. H. Wei and A. Zunger, Phys. Rev. B, 1999, **60**, 5404-5411.